TECHNICAL PAPER

ISSN: 1047-3289 *J. Air & Waste Manage. Assoc.* **61**:1246–1261
DOI: 10.1080/10473289.2011.596741

Simulated Seasonal Variations in Wet Acid Depositions over East Asia

Cui Ge and Meigen Zhang
State Key Laboratory of Atmospheric Boundary Layer Physics and Atmospheric Chemistry, Institute of Atmospheric Physics, Chinese Academy of Sciences, Beijing, People's Republic of China

Lingyun Zhu
Shanxi Province Meteorological Institute, Taiyuan, People's Republic of China

Xiao Han
State Key Laboratory of Atmospheric Boundary Layer Physics and Atmospheric Chemistry, Institute of Atmospheric Physics, Chinese Academy of Sciences, Beijing, People's Republic of China

Jun Wang
Department of Earth and Atmospheric Sciences, University of Nebraska–Lincoln, Lincoln, Nebraska, USA

ABSTRACT
The air quality modeling system Regional Atmospheric Modeling System–Community Multi-scale Air Quality (RAMS-CMAQ) was applied to analyze temporospatial variations in wet acid deposition over East Asia in 2005, and model results obtained on a monthly basis were evaluated against extensive observations, including precipitation amounts at 704 stations and SO_4^{2-}, NO_3^-, and NH_4^+ concentrations in the atmosphere and rainwater at 18 EANET (the Acid Deposition Monitoring Network in East Asia) stations. The comparison shows that the modeling system can reasonably reproduce seasonal precipitation patterns, especially the extensive area of dry conditions in northeast China and north China and the major precipitation zones. For ambient concentrations and wet depositions, the simulated results are in reasonable agreement (within a factor of 2) with observations in most cases, and the major observed features are mostly well reproduced. The analysis of modeled wet deposition distributions indicates that East Asia experiences noticeable variations in its wet deposition patterns throughout the year. In winter, southern China and the coastal areas of the Japan Sea report higher SO_4^{2-} and NO_3^- wet depositions. In spring, elevated SO_4^{2-} and NO_3^- wet depositions are found in northeastern China, southern China, and around the Yangtze River. In summer, a remarkable rise in precipitation in northeastern China, the valleys of the Huaihe and Yangtze rivers, Korea, and Japan leads to a noticeable increase in SO_4^{2-} and NO_3^- wet depositions, whereas in autumn, higher SO_4^{2-} and NO_3^- wet depositions are found around Sichuan Province. Meanwhile, due to the high emission of SO_2, high wet depositions of SO_4^{2-} are found throughout the entire year in the area surrounding Sichuan Province. There is a tendency toward decreasing NO_3^- concentrations in rainwater from China through Korea to Japan in both observed and simulated results, which is a consequence of the influence of the continental outflow from Eurasia. The same tendency is not found for SO_4^{2-}.

IMPLICATIONS
Seasonal variations of wet acidic depositions in East Asia were studied using the air quality modeling system RAMS-CMAQ. The simulated results provide information on transport, transformation, and wet deposition patterns of acidic substances over East Asia. This information can assist decision makers in designing emission regulations, especially for areas that have serious problems with acid depositions.

INTRODUCTION
Acid rain is a popular term for the atmospheric deposition of acidified rain, snow, sleet, hail, acidifying gases, and particles as well as acidified fog and cloud water. The primary precursors to acidity in the troposphere are SO_2 and NO_x and organic compounds that are emitted and subsequently oxidized into more acidic forms through a complex series of interactions involving numerous chemical, meteorological, physical, and biological processes. Acid rain is a particularly important environmental issue in East Asia because this area has experienced extensive industrialization in the last three decades. Emissions of SO_2 and NO_x have increased at significant rates due to the accelerated use of fossil fuels and automobiles.[1–4] In addition, there have been large emission changes, in terms of both levels and types, in this area in recent years. For example, Asian NO_x emissions have increased rapidly since the 1970s, when they contributed only a minor fraction of global emissions, and surpassed emissions from North America and Europe in the mid-1990s.[5] Tonooka[6] estimated that SO_2 and NO_x emissions in China increased by 19% and 31% from 1988 to 1994, respectively. In Japan,

SO_2 emissions slightly decreased, but NO_x emissions increased by 13% during the period from 1987 to 1995. Park estimated that anthropogenic emissions in Korea increased by 34% for SO_2 and by 122% for NO_x during this same period.[7]

Many of the critical issues concerning acid deposition involve its impacts on natural and man-made systems. To assess these impacts, a great deal of effort has been devoted to determining the emissions magnitudes of acid deposition precursors and the distributions of these substances in East Asia through the use of field monitoring and numerical modeling.[8–20]

Although emissions patterns are essential in evaluating existing and potential acid deposition problems, acid rain pollution has not shown significant improvement despite the control measures implemented in recent years. Because acid deposition is basically a secondary pollutant and its precursors can travel long distances before being deposited, an identification of the transformation and transport processes is critical to understanding this phenomenon, particularly in delineating its extent and magnitude in Asia. Because there is still uncertainty in our understanding and modeling ability (e.g., simulated precipitations, related emissions variations, effects of long-range transport, and transformation and deposition mechanisms of S and N compounds in East Asia), these problems require further study. Besides, the relative precipitation contributions of SO_4^{2-} and NO_3^- have changed in accordance with the relative changes in SO_2 and NO_x emissions. Further study is, therefore, warranted to gain insight into the seasonal distributions of wet depositions and the current precipitation levels of NO_3^-/SO_4^{2-}.

The purpose of this study was to apply a comprehensive air quality modeling system to study seasonal variations in wet acid deposition distributions. First, the model system and its inputs are briefly introduced. Then, the spatial and seasonal distribution patterns of wet deposition are analyzed based on the distribution of precipitation and the concentrations of major acidic species (SO_4^{2-}, NO^{3-}), and a comparison is made to monitoring data obtained from Chinese meteorological stations and the Acid Deposition Monitoring Network in East Asia (EANET) stations. Finally, a summary and conclusions are given.

MODEL DESCRIPTION

In this paper, the air quality modeling system Regional Atmospheric Modeling System–Community Multi-scale Air Quality (RAMS-CMAQ)[21] was employed to study the complex sequence of physical and chemical processes involved in acid deposition in East Asia. The RAMS-CMAQ modeling system contains two major components, the Community Multi-scale Air Quality (CMAQ)[22] and the Regional Atmospheric Modeling System (RAMS). This modeling system can simulate concurrently the atmospheric and land processes affecting the transport, transformation, and deposition of air pollutants and their precursors on both regional and urban scales and has been widely applied to address issues regarding tropospheric ozone and anthropogenic aerosols, such as black and organic carbons, SO_4^{2-}, NO_3^-, NH_4^+, and their precursors, in East Asia.[23–25]

CMAQ version 4.6 was employed in this study to account for chemistry in three phases: the gas phase, aerosols (solid or liquid), and the aqueous phase. CMAQ used meteorological fields simulated by RAMS version 6.0 and CMAQ was configured with the chemical mechanism CB05.[26] The Cloud module in CMAQ performs several functions related to cloud physics and chemistry, and three types of clouds are modeled: subgrid convective precipitating clouds, subgrid nonprecipitating clouds, and grid-resolved clouds. The cloud module vertically redistributes pollutants for the subgrid clouds, calculates in-cloud and precipitation scavenging, performs aqueous chemistry, and accumulates wet deposition amounts. To depict aerosol evolution processes in the atmosphere, the Regional Particulate Model (RPM)[27] module was included. In RPM, the particle size distribution is represented as the superposition of three lognormal subdistributions, and the processes of coagulation, particle growth by the addition of new mass, particle formation, dry deposition, scavenging, and aerosol chemistry are included. CMAQ uses a thermodynamic aerosol equilibrium model known as ISORROPIA to calculate the composition and phase state of the Na^+-NH_4^+-Cl^-- SO_4^{2-}- NO_3^--H_2O system in thermodynamic equilibrium with gas-phase precursors.

A general description of RAMS and its capabilities are given in Pielke et al.[28] The current study used the Kain-Fritsch cumulus parameterization scheme[29] (to represent the subgrid-scale convective cumulus) and the Kessler-type microphysics model.[30] The microphysics module was used to simulate mesoscale clouds and precipitation phenomena. The level 2.5 turbulent closure model,[31] the Land Ecosystem Atmosphere Feedback model,[32] and the soil-vegetation model were also used for the simulation.

RAMS modeling was exercised in a four-dimensional data assimilation mode using analysis nudging with reinitialization every 4 days, leaving the first 24 hr as the initialization period. The three-dimensional meteorological fields for RAMS were obtained from the National Centers for Environmental Prediction (NCEP) final analyses data sets and were available every 6 hr with $1^\circ \times 1^\circ$ resolution. Weekly mean sea surface temperatures (SSTs) and observed monthly snow cover information were used as the boundary conditions for RAMS calculations.

The model domain is 6656×5440 km^2 for CMAQ (shown in Figure 1) on a rotated polar stereographic map projection centered at 35°N and 110°E with a 64-km-grid cell. RAMS and CMAQ have the same model height. For RAMS, there are 25 vertical layers in the σ_z coordinates system unequally spaced from the ground to approximately 23 km, with approximately 9 layers concentrated in the lowest 2 km of the atmosphere to resolve the planetary boundary layer. For CMAQ, there are 15 levels, and the lowest 7 layers are the same as those in RAMS; the lowest layer is approximately 100 m.

The anthropogenic emissions and open biomass burning emissions of SO_2, NO_x, NH_3, hydrocarbons, and particles were obtained from the monthly-based emissions inventory, which has a spatial resolution of $0.5^\circ \times 0.5^\circ$.[33] NO_X and ammonia from soil and natural hydrocarbon emissions were extracted from the Global Emissions Inventory Activity (GEIA) $1^\circ \times 1^\circ$ monthly inventory.[34] Aircraft-exhausted and lightning-produced NO_x were derived from the Emission Database for Global Atmospheric Research (EDGAR) $1^\circ \times 1^\circ$ monthly inventory.[35] Volcanic SO_2 emissions were based on

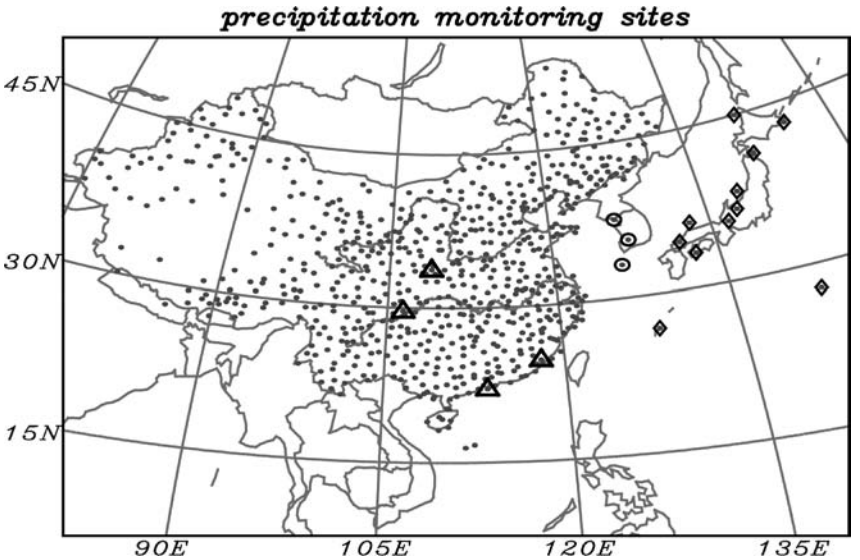

Figure 1. Location of 704 monitoring stations: 704 for precipitation (dot) and 18 for wet deposition (triangles, China stations: Zhuxian, Xiaoping, Jinyunshan, and Jiwozi; circles, Korea: Cheju, Imsil, and Kanghwa; diamonds, Japan: Hedo, Ogasawara, Yusuhara, Ijira, Oki, Happo, Sado, Tappi, Ochiishi, and Rishiri).

the estimates of Streets et al.,[36] and the Miyakejima (2005) estimates provided by the Frontier Research Center for Global Change of Japan.

The boundary conditions and initial conditions for CMAQ were adopted from the outputs of MOZART-4 (Model for Ozone and Related chemical Tracers, version 4).[37]

RESULTS AND DISCUSSION

To analyze the horizontal distribution patterns of acid deposition, RAMS-CMAQ was executed continuously from December 26, 2004, to December 31, 2005. The modeling results were evaluated against actual precipitation amounts observed at 704 rain gauge stations and concentrations of SO_4^{2-}, NO_3^-, and NH_4^+ in the atmosphere and in rainwater observed at 18 EANET stations. The locations of these sites are shown in Figure 1, and some basic information about EANET stations is given in Table 1.

The predominant weather pattern in East Asia is the monsoon system. In the winter (December, January, and February), winds flow clockwise out of the Siberian High, blowing cold, dry air south-southwestward toward the Himalayas and southeastern Asia, north-northeastward to northern Asia, and southeastward to China, Korea, and Japan. In the summer (June, July, and August), moisture-laden winds blow from the Pacific Ocean northwestward into China, Japan, and northern Asia. The period from October to May comprises the winter circulation pattern, typified by January. The period from June to September comprises the summer pattern, typified by July. Spring (March, April, and May) and autumn (September, October, and November) in East Asia correspond to the periods of transition between the winter and summer monsoons. Acid deposition patterns considered on a seasonal mean basis are discussed below.

Table 1. The locations and characteristics of EANET stations.

Station	Country	Category	Latitude (°N)	Longitude (°N)	Height (m)
Jinyunshan	China	Rural	29.82	106.37	800
Jiwozi	China	Remote	33.83	108.80	2100
Xiaoping	China	Remote	24.85	118.03	686
Zhuxian	China	Urban	22.20	113.52	45
Kanghwa	Korea	Rural	37.70	126.28	150
Cheju	Korea	Remote	33.30	126.17	72
Imsil	Korea	Rural	35.60	127.18	0
Rishiri	Japan	Remote	45.12	141.23	40
Ochiishi	Japan	Remote	43.15	145.50	49
Tappi	Japan	Remote	41.25	141.35	105
Ogasawara	Japan	Remote	27.08	142.22	230
Sado	Japan	Remote	38.25	138.40	110
Happo	Japan	Remote	36.68	137.80	1850
Oki	Japan	Remote	36.28	133.18	90
Yusuhara	Japan	Remote	32.73	132.98	225
Hedo	Japan	Remote	26.78	128.23	50
Ijira	Japan	Rural	35.57	136.70	140
Banryu	Japan	Urban	34.67	131.70	60

Seasonal Precipitation Patterns

Precipitation is important for determining the amount of wet deposition. Deposition of SO_4^{2-} and NO_3^- can be coupled to large-scale precipitation-producing weather systems, which deposit these acidic substances farther from emission sources than the same chemicals produced via gaseous-phase (dry) processes. For evaluating the model, simulated seasonal mean precipitation amounts were compared with observations at 704 rain gauge stations, including 681 Chinese meteorological stations and 23 EANET stations. Figure 2 shows both observed and modeled seasonal mean precipitation distributions in the winter, spring,

Table 2. Statistics for observed and modeled monthly averaged precipitation amounts (mm) at 704 stations in 2005.

Month	C_{obs}	C_{model}	σ_{obs}	σ_{model}	NMB (%)	R
1	16.11	11.41	27.84	16.19	−29.24	0.48
2	34.64	17.85	55.62	18.80	−48.56	0.58
3	37.32	25.63	51.70	33.57	−31.38	0.73
4	47.37	46.48	45.71	64.82	−1.88	0.71
5	110.35	134.27	118.36	226.04	21.71	0.76
6	137.30	197.15	149.78	378.23	43.65	0.75
7	135.43	174.40	106.06	194.64	28.82	0.41
8	141.86	174.05	110.25	228.76	22.73	0.47
9	85.11	84.40	92.75	136.11	−0.83	0.52
10	41.81	25.45	49.93	44.11	−39.18	0.54
11	24.82	17.20	41.32	28.39	−30.74	0.63
12	12.85	9.92	22.92	17.03	−22.88	0.74
Yearly	68.75	76.52	95.46	175.67	11.30	0.68

Notes: C_{obs} = total mean of observed monthly precipitations; C_{model} = total mean of modeled monthly precipitations; σ_{obs} = standard deviation of observed monthly precipitations; σ_{model} = standard deviation of modeled monthly precipitations; NMB = normalized mean bias; R = correlation coefficient between observed and modeled precipitations.

summer, and autumn of 2005. Statistical comparisons of the results are summarized in Table 2. The observed values in Figure 2 were averaged without interpolation for stations located in the same grid. The differences between simulated and observed seasonal mean precipitation amounts for the four seasons are showed in Figure 3.

As shown in Figure 2, the general features of climatological precipitation patterns in all four seasons in China, characterized by a gradual decrease of precipitation from southeast to northwest, were well reproduced. In all four seasons, the western part of north China held the lowest precipitation value in East Asia, which corresponds to semiarid or grassland climate zones.[38] Only in summer did this area receive any amount of rainfall, which was still less than 10 mm in most areas, as shown in Figure 2c. The extensive areas of dry conditions in northeast China and north China and the major precipitation zones were also well simulated for all four seasons. Seasonal precipitation variations were particularly high in East Asia, with maximum magnitudes occurring in summer, autumn, and spring, whereas the lowest magnitudes were observed in winter; these features were reproduced reasonably well by the modeling system. Predictive accuracies were relatively high in northwest China, most of North China, the Big Bend of the Yellow River, Xinjiang, and some regions between the low reaches of the Yellow and Yangtze rivers (Figure 3). However, major discrepancies between the modeled results and observations were found for the southern part of China. In winter, the modeling system underestimated the precipitation over the southern part of China, and precipitation levels in the other three seasons were overestimated by varying degrees. Such overestimated precipitation values were also reported by Ding Yi hui,[38] who found that although the regional climate model RegCM_NCC was capable of predicting the major seasonal rain belts, precipitation amounts were significantly overestimated, especially in the southern part of China (where error percentages were 80–200%). Similar overestimations of precipitation levels were also reported by Kato et al.[39] and Lee and Suh[40] for East Asia and by Small et al.[41] for central Asia. As suggested by Leung et al.,[42] this deficiency is likely to be predominantly associated with the cloud-radiation transfer parameterization.

The accuracy of the model varies from season to season, with the highest accuracy in April (NMB of −1.88% and R of 0.71) and the lowest in February (NMB of −48.56% and R of 0.58). In winter, East Asia is under the influence of the winter monsoon due to strong pressure gradients between the Siberian high-pressure systems over the East Asian continent and the low-pressure systems over the North Pacific. With the exception of southern China, precipitation levels were very low for China but were substantial for the coastal areas of the Japan Sea (Figure 2a and e). Rainfall levels in southern China and the coastal areas of the Japan Sea were well reproduced by the model. Values larger than 100 mm were observed over the northwest coastal areas of Japan, a feature that was modeled with comparable magnitude. However, the model underestimated precipitation levels in the southern region of the Yangtze River valley (Figures 2 and 3), and as a result, the modeled precipitation levels in winter (December, January, and February) were less than those observed (cf. Table 2).

Spring is the period of transition between the winter and summer monsoons in East Asia and exhibits elevated precipitation levels in southeastern China and northeastern China (Figure 2b). The simulated results (Figure 2f) in most areas of China were consistent with observations with regard to both patterns and magnitudes (e.g., in the north of China and along the Yellow River), whereas the model overpredicted the amount of precipitation in southern China. Table 2 shows that the modeling system can effectively reproduce spring rainfall patterns and levels. The total average monthly precipitation levels obtained by the model are in good agreement with those observed at 704 stations in March, April, and May. Moreover, the correlation coefficients between observed and modeled precipitation data are all larger than 0.70.

The summer monsoon brought wet and warm marine air to the continent from the India Ocean and the West Pacific, causing significant precipitation, particularly near the coast, where marine air and continental air interface. As shown by Figure 2c and g, the model effectively reproduces the sufficient summer precipitation levels in the low-latitude region. In the continental area, the highest summer precipitation levels occurred in northeastern China, the Huaihe River valley, along the Yangtze River, the coastal regions of Southeast China, Korea, and southern Japan, with maximum precipitation levels reaching 300 mm or more. Figure 2c and g also show that the summer was characterized by a large of amount of precipitation in the Huaihe Basin (located in the middle of eastern China, about midway between the Yellow River and the Yangtze River) and relative dry conditions in the southern region of the Yangtze River valley. The model generally captured these major features but overestimated precipitation levels in the Guangdong, Guangxi, and Jiangxi provinces. In addition, the model underpredicted the precipitation over southwestern China in the eastern and southern foothills

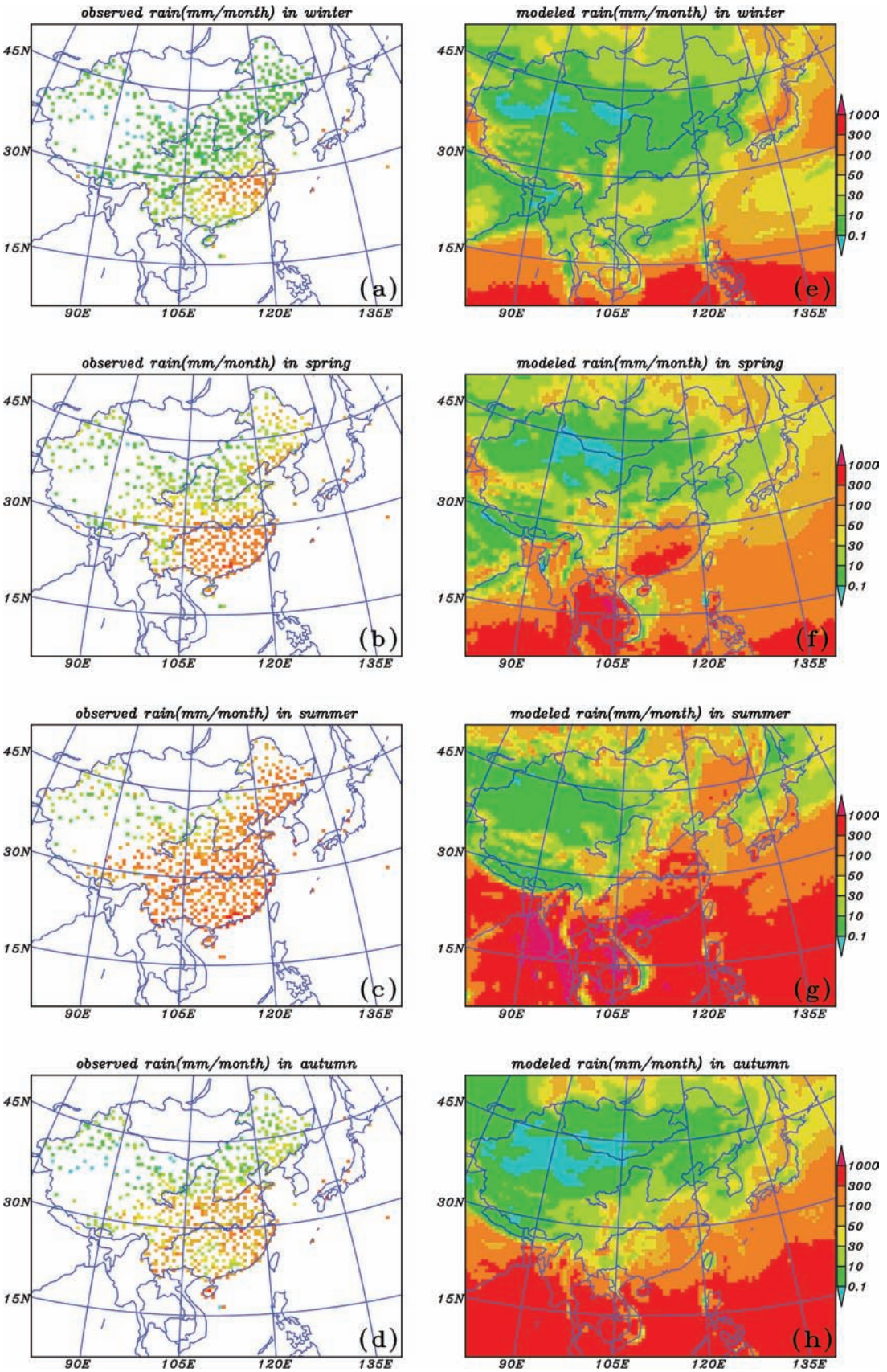

Figure 2. Observed seasonal mean precipitation amounts (mm/month) for (a) winter (December–February), (b) spring (March–May), (c) summer (June–August), and (d) autumn (September–November) of 2005; and simulated seasonal mean precipitation amounts (mm/month) for (e) winter (December–February), (f) spring (March–May), (g) summer (June–August), and (h) autumn (September–November) of 2005.

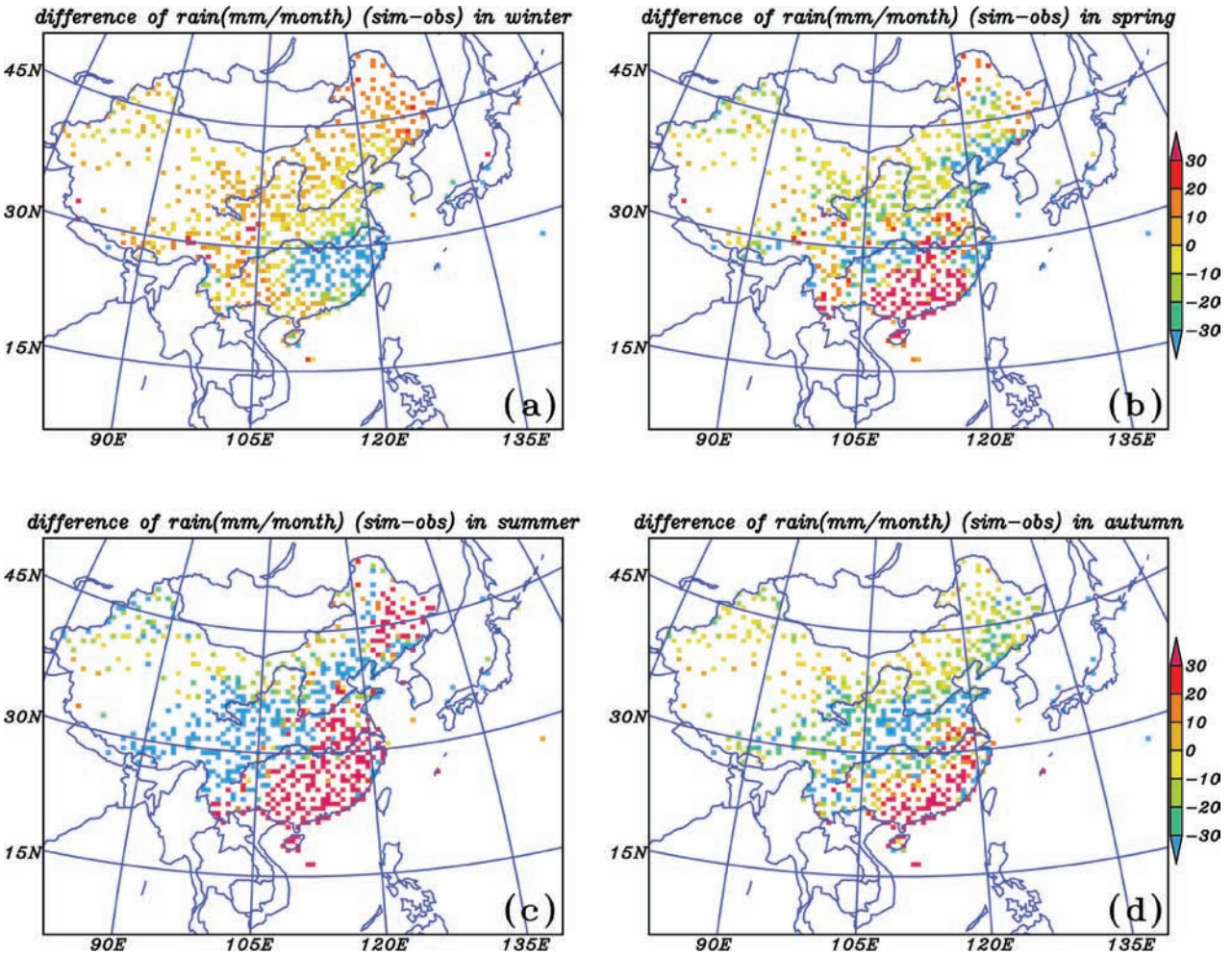

Figure 3. Differences between simulated and observed seasonal mean precipitation amounts (mm/month) for (a) winter (December–February), (b) spring (March–May), (c) summer (June–August), and (d) autumn (September–November) of 2005.

of the substantial Tibetan Plateau, where the existence of complex terrain features may cause unrealistic results.[38]

Autumn is a dry season in East Asia, and it is a transition period just like spring. Nonetheless, autumn still exhibited substantial rainfall over low-latitude areas in which the rain zone withdrew toward to equator. Both the observations and the simulations obtained for the continental area of East Asia, in general, displayed a downward precipitation trend in October compared to April, especially over the northeast edge of China and the coastal regions of Southeast China. The exceptions were Yunnan Province and the upper Yangtze River valley, in which October precipitation levels were above 100 mm, much higher than those observed in April for the same regions. The simulated pattern generally corresponds well with the observed one, but the model underpredicted October precipitation levels in the central area between the Yellow River and the Yangtze River.

Seasonal Ambient Concentration Distributions of SO_4^{2-} and NO_3^-

Winter emission distributions of SO_2 and NO_x and the difference emission distributions between summer and winter for SO_2 and NO_x are shown in Figure 4. Large spatial variations (in the emission rates) were found for both SO_2 and NO_x in East Asia. Large SO_2 emissions can be seen in the Sichuan Basin, industrialized eastern China, and the volcano eruption over the Miyakejima area (located south of Tokyo, Japan). Higher NO_x emissions are found in northern China, the region between the Yangtze River and the Yellow River, and the coastal region of southern China. The relatively strong NO_x signature that results from transportation sources in Japan is also depicted in Figure 4. East Asia, especially China, has an apparent seasonality of emissions for both SO_2 and NO_x, with maximum emissions occurring in wintertime (the heating period).[36] Because residential heating increases in winter, higher SO_2 emissions can be seen over central eastern China and the Sichuan Basin. Emission levels of NO_x in northern China are also larger in winter compared to summer.

Figure 5 shows the observed and simulated monthly averaged ambient concentrations of SO_4^{2-}, NO_3^-, and NH_4^+ obtained from 10 EANET stations located in Japan (see Figure 1 and Table 1 for station locations and categories). The ambient concentrations of SO_4^{2-} were between 0.08 and 11.32 $\mu g\ m^{-3}$, whereas both NO_3^- and NH_4^+

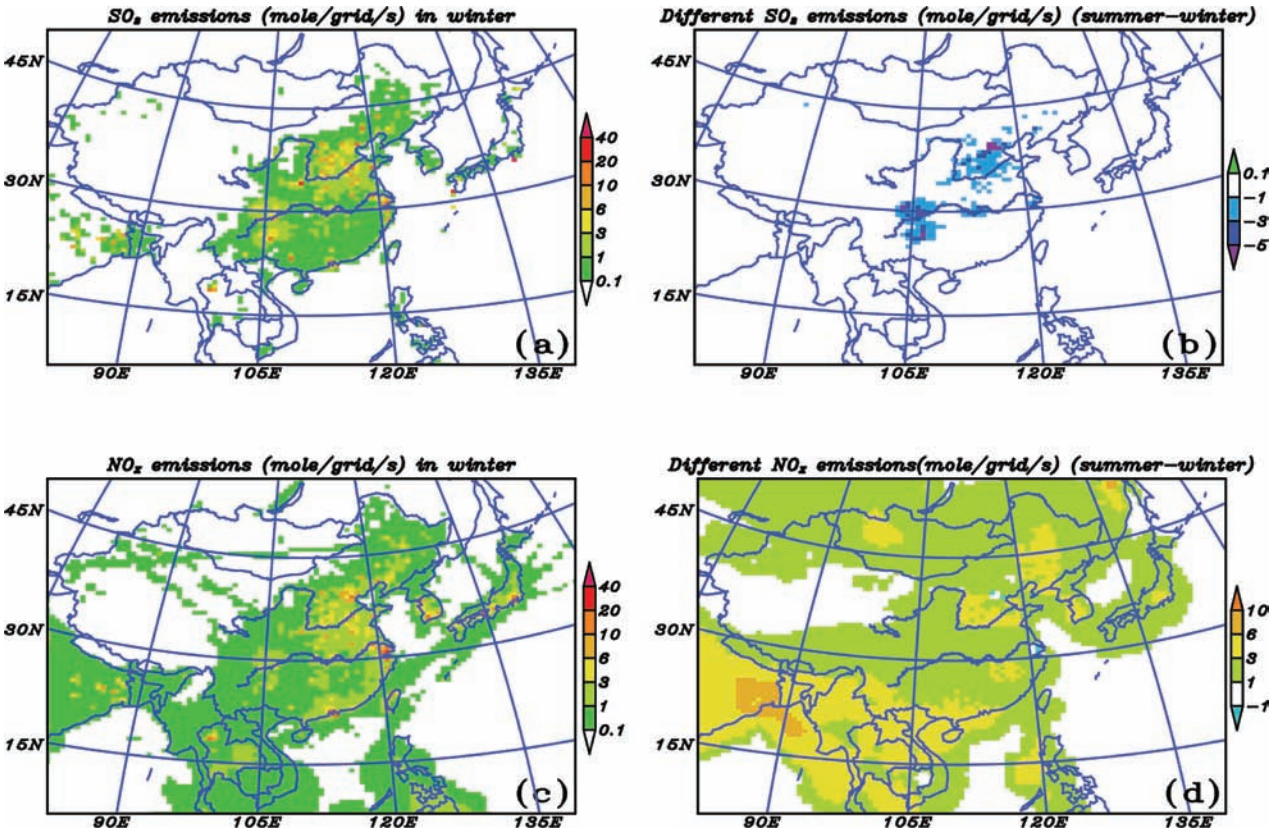

Figure 4. Emissions distributions in winter for (a) SO_2 and (c) NO_x (mole/grid/s). And the difference between summer and winter emissions distributions for (b) SO_2 and (d) NO_x.

concentrations were comparatively lower (between 0.01 and 2.82 μg m^{-3} for NO_3^- and between 0.01 and 3.25 μg m^{-3} for NH_4^+). The simulated magnitudes for all three ions were consistent with observations.

Figure 5 shows that the concentrations of all three ambient ions exhibit strong spatial variations, with the highest maximums occurring at Banryu and Ijira and the smaller maximums occurring at Ogasawara. Ogasawara is located on isolated islands in the western Pacific (cf. Figure 1) that are slightly affected by local and domestic emissions from distant mega-city source regions. The levels of SO_4^{2-}, NO_3^-, and NH_4^+ in Ogasawara are the lowest of all 10 stations studied. Oki, Yusuhara, and Hedo are all remote sites, but they are often under the influence of continental anthropogenic emissions and volcano exhausts. Thus, their SO_4^{2-}, NO_3^-, and NH_4^+ levels do not differ significantly from those observed at Banryu and Ijira, which are urban and rural sites. Like Ogasawara, Hedo is a remote oceanic site that is influenced by continental outflow; thus, the species levels are lower for Hedo compared to Oki and Yusuhara, though they are still much higher in Hedo than in Ogasawara. Lower concentrations of these species are observed on Rishiri Island because it is located near the northern tip of Japan, which is dominated by background conditions; except for the outbreaks of Eurasian continental air pollution that occur in spring, SO_4^{2-} and NO_3^- concentrations over Rishiri Island are usually very low and, in fact, are comparable to those observed over the remote ocean.[43]

Figure 5 shows that, in general, the model reasonably reproduced the monthly variations and spatial variations recorded at most stations. In this regard, at all 10 stations, the three species showed strong seasonal cycles with elevated values in the spring that are associated with the Asian winter monsoon season and the transport of pollutions from the Eurasian continent. Both observed and simulated SO_4^{2-} concentrations also peak in summertime, as reported by Carmichael at Cheju Island in Korea.[44] Observed and simulated NO_3^- levels both display minimums in summer, but the model overpredicted the levels observed during spring and winter. The seasonal cycles of SO_4^{2-} and NO_3^- are analyzed and discussed below. Observed NH_4^+ levels show a maximum in summer, a pattern reflected in the simulated results; however, the model overpredicted the actual NH_4^+ concentrations. During the 5-year period from 1982 to 1986, Yamamoto found a distinct seasonal trend in which NH_3 concentrations peaked in summer at an urban site in Yokohama, Japan,[45] and reported a good correlation between diurnal NH_3 concentrations and average air temperatures during the 5-year period. Carmichael also reported that NH_4^+ concentrations tended toward a maximum in late spring-early summer at Cheju Island, Korea; his study suggests that high NH_4^+ values in summer may reflect the strong temperature dependency of NH_3 emissions.[44]

Figures 6 and 7 show simulated the seasonal mean SO_4^{2-} and NO_3^- concentration distributions in the boundary layer (from the surface to ~1000 m) for winter, spring,

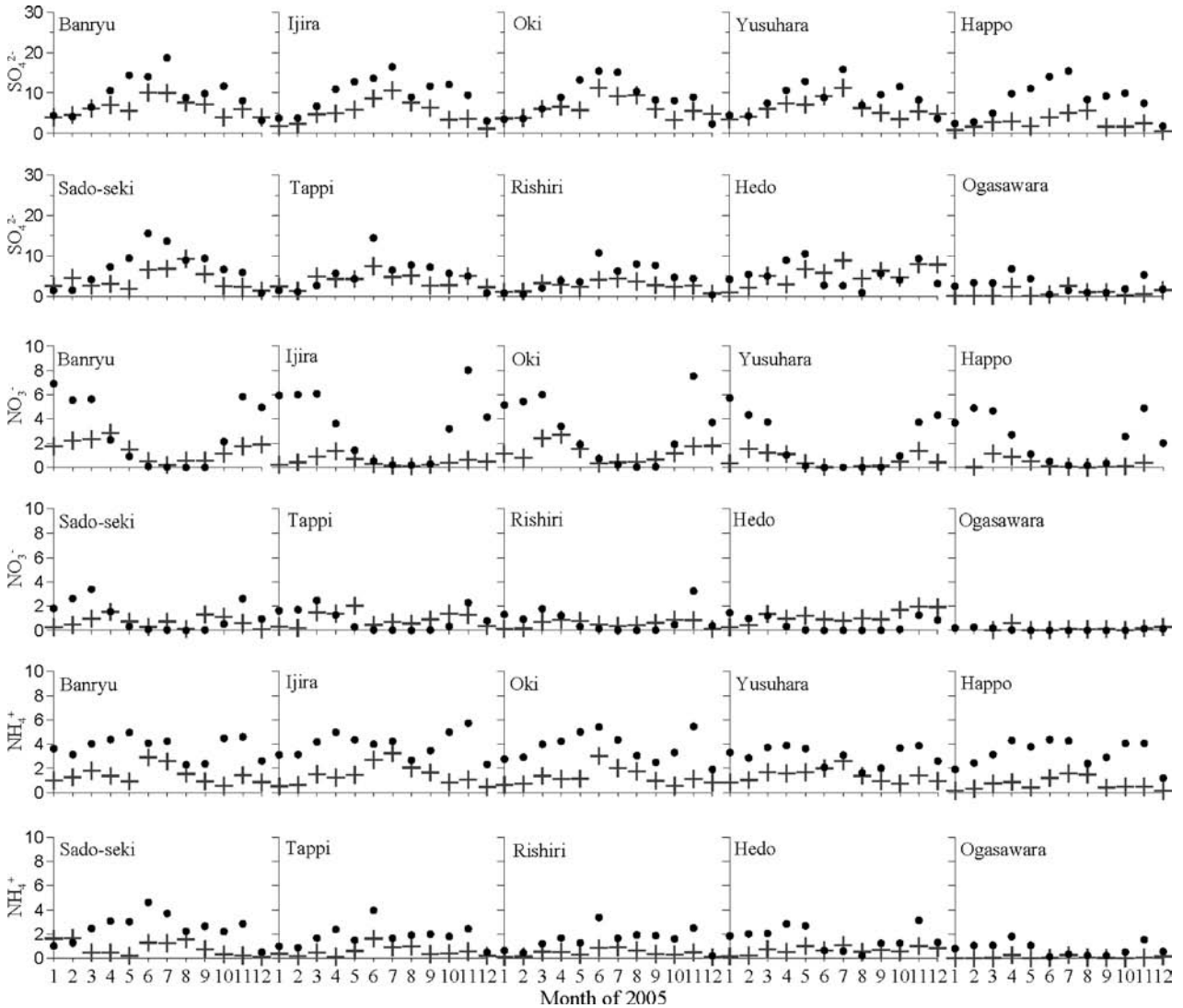

Figure 5. Monthly averaged observed (cross) and simulated (dot) concentrations of SO_4^{2-}, NO_3^-, and NH_4^+ ($\mu g\ m^{-3}$) at 10 EANET stations in Japan.

summer, and autumn in 2005. Seasonal mean wind vectors at an altitude of approximately 500 m are also shown in Figure 6. Throughout the entire year, the maximum SO_4^{2-} concentrations are found in the area surrounding Sichuan Province (Figure 6). This feature is attributed to both emissions and meteorological conditions. SO_4^{2-} is primarily produced from the oxidation of SO_2, and the conversion of SO_2 to SO_4^{2-} occurs via multiple pathways, including gas-phase oxidation to H_2SO_4 followed by condensation into the particulate phase, aqueous-phase oxidation in cloud or fog droplets, and various reactions on the surfaces or inside aerosol particles. Sichuan has higher SO_2 emissions (Figure 4), and the Sichuan Basin is enclosed on four sides by mountains and the Yunnan-Guizhou Plateau. Due to the seasonally variant, high frequency of calm winds and their temperature inversion strength, air pollutants have difficulties diluting in the Sichuan Basin. As a result, a large number of pollutants accumulate in the Sichuan Basin.

Figure 6a shows that elevated SO_4^{2-} concentrations ($\geq$30 $\mu g\ m^{-3}$) in winter are mainly found over central China. Because they are controlled by the Siberian High, the surface winds are initially northeastwards in northern China, Japan, and Korea, then they flow clockwise out to sea and move southwards along the coast into the South China Sea. This wind pattern brings large amounts of surface pollutants that originate in the boundary layers of Eurasia to the West Pacific Ocean, the South China Sea, and the Indian Ocean. Because temperature and water contents along this transport path are relatively high, SO_2 transported from the Asian continent can be quickly oxidized in the gas phase and the aqueous phase, producing a wide area in which SO_4^{2-} concentrations larger than 10 $\mu g\ m^{-3}$ spread south and even expand to 10°N.

Spring in East Asia is the period of transition between the winter and summer monsoons. As shown in Figure 6b, in eastern China the southwesterly winds south of 35°N sweep the pollution northeastward. Thus, high SO_4^{2-} concentrations ($\geq$30 $\mu g\ m^{-3}$) are found along the transport path from Hunan Province through Hubei Province to the convergence zone between 30°N and 40°N, where air

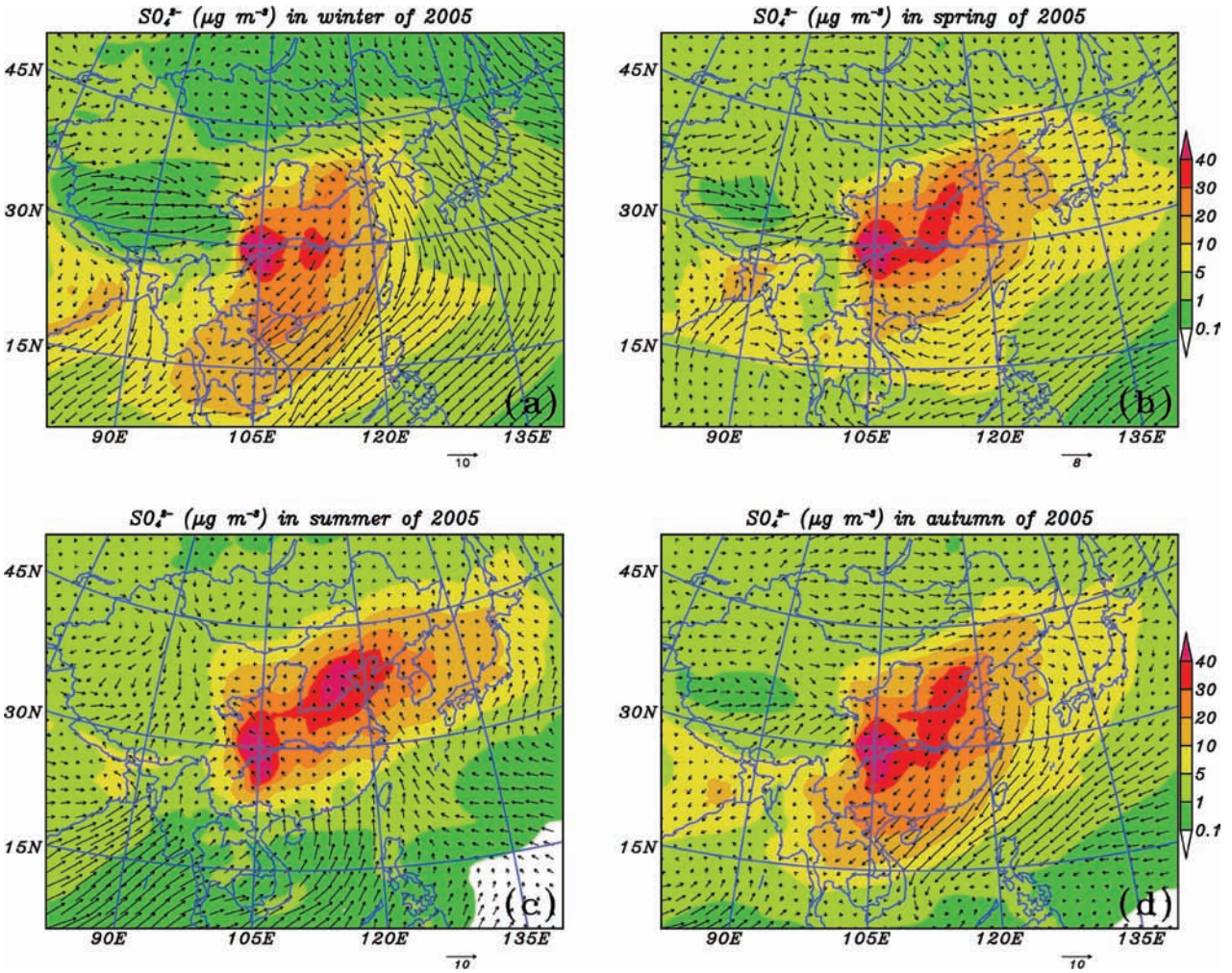

Figure 6. Horizontal distributions of seasonal mean SO_4^{2-} (μg m^{-3}) concentrations in the boundary layer (from surface to about 1000 m) in (a) winter (December–February), (b) spring (March–May), (c) summer (June–August), and (d) autumn (September–November) of 2005. Also shown are seasonal mean wind vectors at approximately 500 m.

masses from the north encounter oceanic air from the south. This pollution is continually transported to the Yellow Sea, Korean peninsula, and Japan. It can be seen that the convergence zone over central and eastern China plays an important role in the springtime export of pollution from the Asian continent, as reported by Zhang et al.[23]

In summer, the prevailing wind is from the south and southeast (onshore wind). The southern part of China in the boundary layer is affected by the summer monsoon; thus, SO_4^{2-} concentrations smaller than 10 μg m^{-3} are observed in most areas of southern China due to the deep boundary layer, deep convection, and mixing with low-latitude marine air. The SO_4^{2-} values around the area of Sichuan Province are higher than 40 μg m^{-3} throughout the year. In northern China, the areas of SO_4^{2-} in summer are higher than 40 μg m^{-3}, which is larger than that observed during other seasons, due to both the higher production of SO_4^{2-} from SO_2 and meteorological conditions in summer. In summer, the water vapor content is elevated, and the wet marine monsoon produces higher [OH], resulting in a higher formation rate of SO_4^{2-} from SO_2. The southerly winds push pollution northwards and then northeastwards, resulting in a SO_4^{2-} maximum in the Beijing-Tianjin-Hebei region, the Bay of the Bohai Sea, and Korea. Influenced by transportation from China, in summer the concentrations of SO_4^{2-} in most areas of Japan are higher than 10 μg m^{-3}, as seen in Figure 4. Compared to other seasons, Japan is most strongly influenced in summer by pollution originating over the Asian continent.

The general flow field in autumn is shown in Figure 6d. Westerly and southwesterly winds prevail north of 40°N, and there are anticyclone circulations over central and eastern China. Following this wind flow, much of the pollution originating in central and eastern China flows clockwise along the coastal area of China and then returns to the south of China. As a result, in autumn, much of the pollutants were trapped in China, with higher SO_4^{2-} concentrations (≥30 μg m^{-3}) over southern China, and a smaller amount of SO_4^{2-} was transported to the western Pacific compared to spring.

Figure 7 shows that, throughout the year, the higher NO_3^- concentrations were generally found between the Yangtze River and the Yellow River because this area is characterized by high emissions of NO_x and NH_3.[34,36]

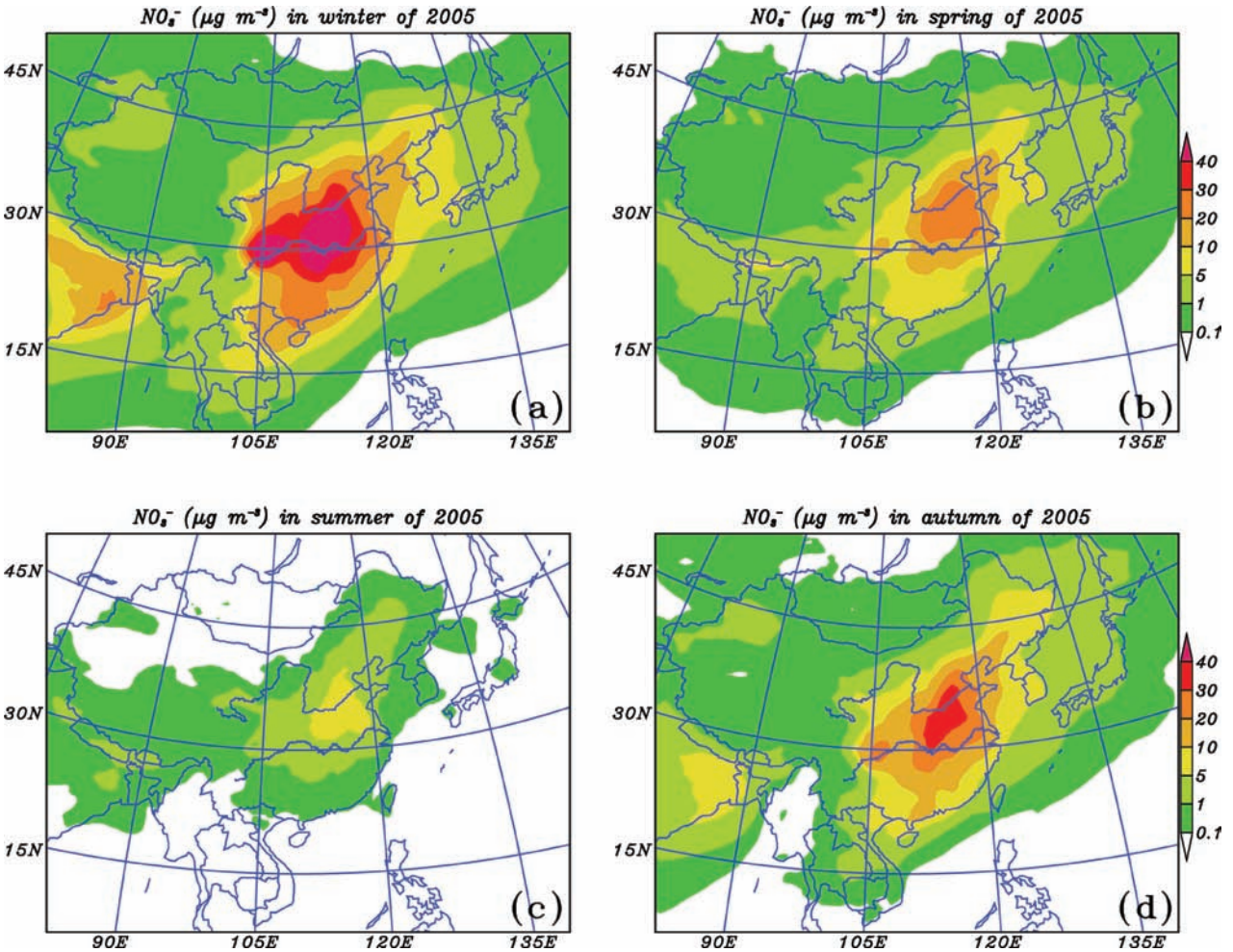

Figure 7. Horizontal distributions of seasonal mean NO_3^- ($\mu g\ m^{-3}$) concentrations in the boundary layer (from surface to about 1000 m) in (a) winter (December–February), (b) spring (March–May), (c) summer (June–August), and (d) autumn (September–November) of 2005.

Following the monsoon transition process, the location of the maximum NO_3^- moved north from spring to summer and moved south in autumn, similar to the pattern observed for SO_4^{2-}. There is an obvious difference between the distribution patterns of NO_3^- with SO_4^{2-}, in that the higher SO_4^{2-} concentrations are all approximately 30 $\mu g\ m^{-3}$ for all four seasons, whereas maximal NO_3^- concentrations have noticeable differences that depend on seasonal changes. Generally, the NO_3^- concentrations are higher in winter and autumn, lower in spring, and lowest in summer. The highest NO_3^- concentrations vary seasonally by a factor of approximately 4 with a maximum in winter ($\geq$40 $\mu g\ m^{-3}$) and a minimum in summer ($\geq$10 $\mu g\ m^{-3}$). In the model, NO_3^- is produced from NO_x, and NO_3^- aerosols and is normally present as particulate NH_4NO_3, formed from the reversible reaction of gas-phase NH_3 and HNO_3. Because HNO_3 is easily absorbed by rainwater and cloud-water, the concentration of NO_3^- is heavily influenced by both temperature and precipitation.

Figure 7a shows that, in winter, the transport of NO_3^- had a smaller impact over downwind marine areas than SO_4^{2-} because when NO_3^- is transported to the oceanic area, its concentration decreases very quickly. Significant gradients exist from eastern China through the coastal area to the West Pacific, with the 30 $\mu g\ m^{-3}$ starting concentration of NO_3^- decreasing to less than 0.1 $\mu g\ m^{-3}$. From Figure 7b, we can see that the NO_3^- concentrations decrease sharply from winter to spring and that high NO_3^- concentrations are found around the Huaihe valley with a maximum lower than 30 $\mu g\ m^{-3}$. The highest concentration decreased in summer to below 10 $\mu g\ m^{-3}$. Figure 6d also shows that the higher NO_3^- concentration found in autumn corresponds to the area over the Huaihe valley, with a highest concentration larger than 30 $\mu g\ m^{-3}$.

Figures 6 and 7 also show that most regions of Asia have higher concentrations of SO_4^{2-} than NO_3^-, although NO_3^- concentrations are a little higher than SO_4^{2-} concentrations in some regions (e.g., in eastern China and northeastern China in the winter time), suggesting a greater importance of NO_x emission in these regions. Since 1996, SO_2 emissions in China have slowly declined[46] because of measures such as restrictions on the use of coal-fired household stoves, the termination or relocation of heavily polluting industries in urban areas to the countryside, and the installation of scrubbers on coal-fired boilers. Many researchers agree that the rapid growth of the

transportation sector in Asia has caused NO_x emissions to climb steeply. For example, the number of motor vehicles in China has increased dramatically in recent years from 6.2 million in 1990 to 36.0 million in 2003. The corresponding changes in SO_2 and NO_x emissions are significant in that they may considerably alter the relative levels of NO_3^- and SO_4^{2-} in precipitation in East Asia. The typical type of sulfuric acid in Asia is changing, and these changes have aroused serious concerns in public and government sectors.

Seasonal Wet Deposition Distributions of SO_4^{2-} and NO_3^-

Figure 8 compares modeled and observed monthly mean concentrations of SO_4^{2-}, NO_3^-, and NH_4^+ in precipitation observed at the 18 EANET stations. Most of the scatters fall within the reference lines within a factor of 2, whereas some discrepancies occur for some sites. In addition to the uncertainties in related meteorology for aerosol formation, such as the uncertainty of simulated precipitation fields, there are several explanations for the discrepancy. For example, some uncertainties exist in the model treatments that govern the processes for nitrate formation, including thermodynamic equilibrium and gas-to-particle partitioning between gaseous HNO_3 and aerosol nitrate.[47,48] Asian emissions of NH_3 (2006), which play a key role in gas/aerosol partitioning,[36] carry a significant uncertainty linked to the use of European-based emission factors (especially livestock).

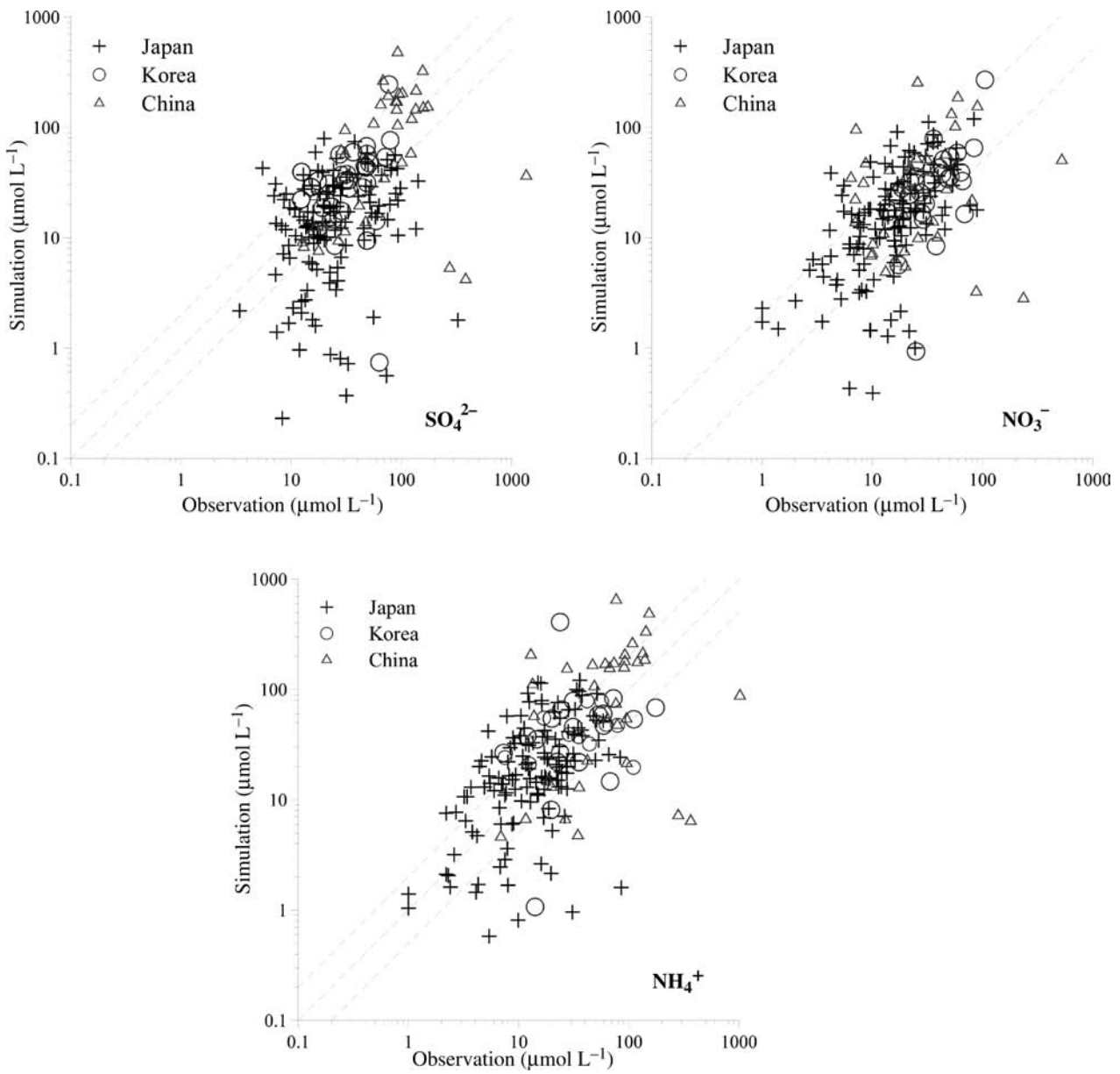

Figure 8. Scatter plots of observed versus modeled monthly averaged contents (μmole L^{-1}) of (a) SO_4^{2-}, (b) NO_3^-, and (c) NH_4^+ in precipitation at 18 EANET stations.

Table 3. Yearly averaged mixing ratios (μmole/L) of SO_4^{2-}, NO_3^-, and NH_4^+ in precipitation at 18 EANET stations in 2005.

	SO_4^{2-}		NO_3^-		NH_4^+	
Station	**Obs**	**Sim**	**Obs**	**Sim**	**Obs**	**Sim**
Jinyunshan	240.7	183.0	95.5	70.9	218.2	212.5
Jiwozi	121.2	119.0	9.8	35.2	43.5	132.4
Xiaoping	29.2	29.9	28.6	22.1	46.8	50.8
Zhuxian	54.5	46.0	35.2	41.7	47.1	63.3
Kanghwa	54.2	58.7	61.0	61.3	64.0	85.4
Cheju	38.3	29.0	32.1	23.5	32.0	33.2
Imsil	27.2	31.9	32.8	33.5	44.9	43.7
Rishiri	30.4	16.0	14.8	15.1	21.8	22.2
Ochiishi	31.9	8.5	12.5	9.2	10.0	11.2
Tappi	51.4	16.3	28.1	15.6	23.6	20.5
Ogasawara	14.6	8.1	4.3	5.9	4.6	9.7
Sado	44.9	32.2	25.9	39.0	27.1	46.7
Happo	16.7	18.3	13.2	17.8	15.1	19.7
Oki	55.9	27.5	28.0	44.4	19.3	50.5
Yusuhara	15.9	18.6	14.9	20.4	11.6	22.6
Hedo	59.3	14.5	13.2	10.5	19.2	19.0
Ijira	20.6	21.9	25.6	24.7	20.9	24.5
Banryu	36.7	29.7	36.0	41.2	26.3	47.7
Total	52.4	39.4	28.4	29.6	38.7	50.9

Table 3 compares yearly averaged mixing ratios in rainwater for the three major ions at 18 EANET stations. For the annual averages obtained for the 18 stations, the simulations reasonably fit the observations for NO_3^- and NH_4^+, particularly for the stations located in Japan and Korea. However, the wet deposition of SO_4^{2-} is substantially underestimated for some stations in China and Japan. Underestimates of SO_2 from volcano emissions in Japan may contribute to the underprediction of wet deposition for SO_4^{2-} in Japan. Volcanoes are significant sources of SO_2 emissions in Japan. There are several large active volcanoes; for example, Sakurajima emitted the largest amount of S toward the end of the 1980s, and Miyakejima erupted in late August of 2000. Volcanic emissions were comparable to anthropogenic emissions in Japan.[49] Ikeda and Higashino[50] and Ichikawa et al.[51] estimated the annual wet deposition of SO_4^{2-} in Japan in 1990, and their results indicated that the contribution of domestic anthropogenic emissions to SO_4^{2-} wet deposition in Japan was only approximately 30%, with the rest of the SO_4^{2-} wet deposition originating from volcanoes located in Japan (estimated contribution of 20–30%) and emission sources outside Japan. Unfortunately, there is little reliable information revealing the temporal trends of SO_2 emissions from these volcanoes.

Table 3 also shows a decreasing tendency in NO_3^- and NH_4^+ mixing ratios in rainwater from China through Korea to Japan in both the observed and simulated results, indicating the influence of continental outflow from Eurasia. At all of the stations except the one in Banryu, the mixing ratios in rainwater for NO_3^- and NH_4^+ in Japan are much less than those in Korea. This tendency is not found for SO_4^{2-}. The average magnitude of observed SO_4^{2-} in rainfall in Korea is 39.9 μmole/L, the SO_4^{2-} concentrations in Hedo, Oki, Tappi, and Sado are more than 44.9 μmole/L, and there are three stations in Japan in which the SO_4^{2-} concentrations in precipitation are higher than 50 μmole/L (Tappi, 51.4 μmole/L; Oki, 55.9 μmole/L; Hedo, 59.3 μmole/L).

Figures 9 and 10 present the spatial distributions of simulated wet deposition in East Asia in winter, spring, summer, and autumn. They clearly show that East Asia experiences noticeable variations of wet deposition during different seasons.

The wet-deposition distribution patterns for both SO_4^{2-} and NO_3^- appear to be more dependent on meteorological conditions, particularly with regard to rain belt and wind flow patterns. From winter to summer, as the rain belt moved northward (Figures 2 and 3) and the pollution was swept northeastward (Figures 5 and 6), the highest SO_4^{2-} and NO_3^- wet depositions responded and moved northeastward, as seen in Figures 9 and 10. In winter, southern China and the coastal areas of the Japan Sea held the higher SO_4^{2-} and NO_3^- wet deposition concentrations. In the western coastal areas of the Japan Sea, wet deposition levels of NO_{3-} (>12 millimole m^{-2} $month^{-1}$) were higher than those of SO_4^{2-}. In spring, elevated SO_4^{2-} and NO_3^- wet deposition levels were found in northeastern China, southern China, and around the Yangtze River. In summer, a remarkable rise of precipitation in northeast China, the valleys of the Huaihe and Yangtze rivers, Korea, and Japan lead to a noticeable increase in SO_4^{2-} and NO_{3-} wet deposition concentrations. In autumn, the higher SO_4^{2-} and NO_{3-} wet deposition levels were found around Sichuan Province. Meanwhile, due to the high emissions of SO_2, high wet deposition levels of SO_4^{2-} were found in the area surrounding Sichuan Province throughout the entire year.

The values of NO_3^-/SO_4^{2-} in precipitation are useful for evaluating the relative contributions of SO_4^2 and NO_3^- to the acidity of precipitation. Figures 9 and 10 show that the acid rain occurring over most of Asia is a typical sulfate-kind characterized by a higher wet deposition of SO_4^{2-} and a lower wet deposition of NO_3^-,[46] although in some regions the wet deposition of NO_3^- is somewhat higher than that of SO_4^{2-}. A ratio of 1.0 was found around the Taiwan Strait and the Tokyo district throughout the entire year, and a ratio of 2 was determined in winter, indicating that these areas are substantially affected by large NO_x emissions. There are also other areas in which NO_3^- has significantly contributed to acid rain. In spring and autumn, a ratio of 1.0 mainly occurred in the areas around or downwind of big cities or industrial regions, such as some parts of north China, the Pearl River Delta, the Taiwan Strait, the Tokyo district, Korea, and a large area around the Japan Sea. In winter, a ratio of 1.0 is found for most of southeastern China. Takahashi and Fujita[9] studied the results of six sites in western Japan from 1987 to 1996 and found a higher rate of NO_x emissions than SO_2 emissions that may considerably alter the relative strengths of nitrate and sulfate in precipitation in this area.

SUMMARY AND CONCLUSION

Seasonal variations of wet acidic depositions in East Asia were studied by the air quality modeling system RAMS-CMAQ. Results for the year of 2005 were simulated, and the seasonal distribution patterns of wet deposition were

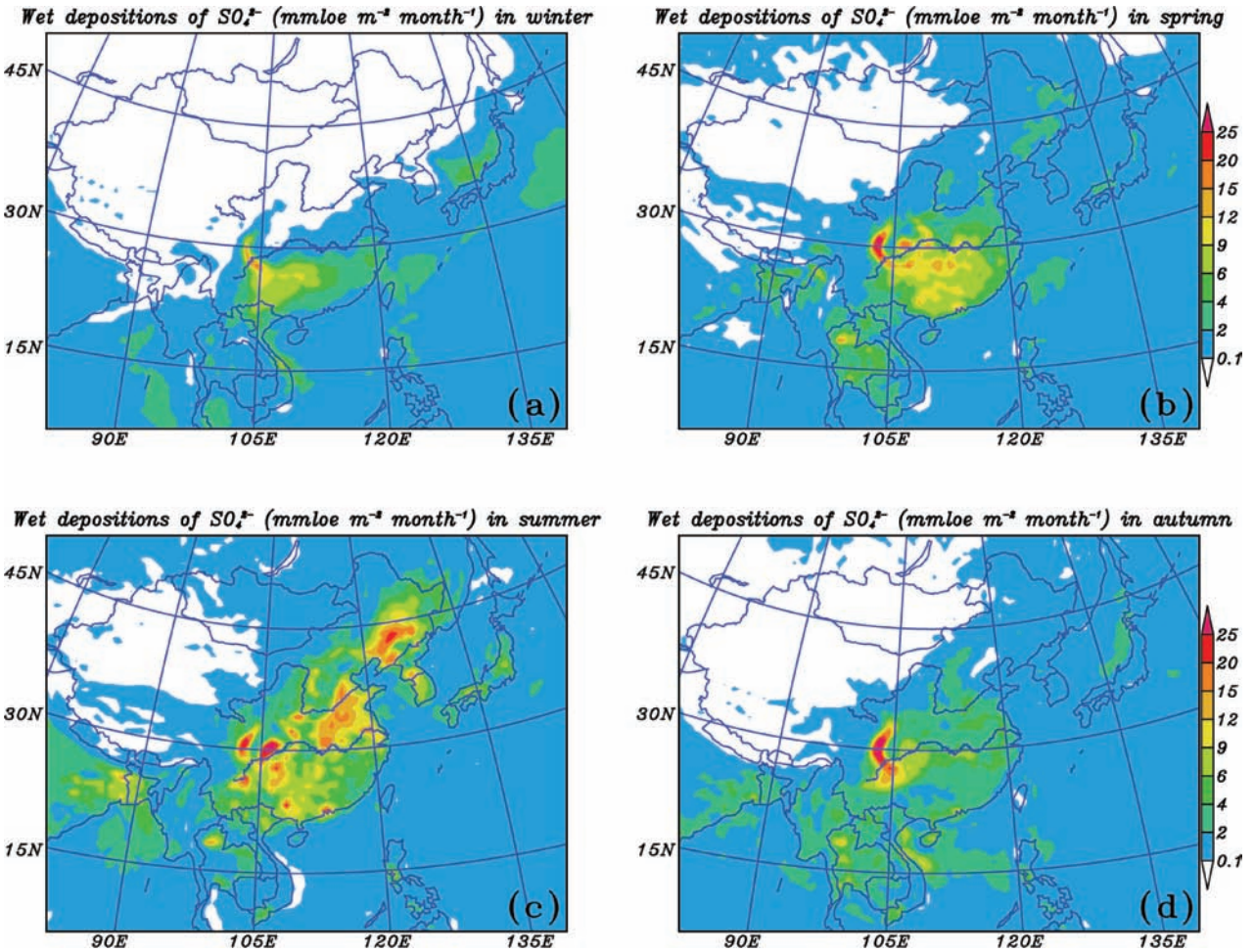

Figure 9. Modeled wet deposition fluxes (m mole m^{-2} $month^{-1}$) of SO_4^{2-} in (a) winter (December–February), (b) spring (March–May), (c) summer (June–August), and (d) autumn (September–November) of 2005.

analyzed based on the distribution of precipitation and the major acidic species (SO_4^{2-} and NO_3^-). In addition, the simulated results were compared to extensive observations, including monthly precipitation amounts from 704 stations, monthly averaged ambient aerosol concentrations of SO_4^2, NO_3^-, and NH_4^+ at 10 EANET stations and ion concentrations of SO_4^2, NO_3^-, and NH_4^+ in rainwater at 18 EANET stations.

Comparisons of the simulated and observed fields for winter, spring, summer, and autumn show that the modeling system was capable of effectively simulating the major seasonal rain belts and dry areas and showed magnitudes comparable to the observations. Spring was the best-predicted season, as indicated by its high correlation coefficient (>0.70), whereas other months depicted discrepancies in simulated precipitation for southern China. Comparison of model results with observations in terms of the concentrations of the relevant acidic species (SO_4^{2-}, NO_3^-, and NH_4^+) and major ionic species in rainfall showed that, in general, the simulation could reproduce the major features observed for wet deposition and yield reasonable results (within a factor of 2) compared to observations in most cases.

The monthly averaged SO_4^{2-} and NO_3^- distributions in the boundary layer(s) for winter, spring, summer, and autumn in 2005 were also analyzed. Throughout the year, the maximum concentrations of SO_4^{2-} were found in the area of Sichuan Province due to the high-S-content coal utilized and the special geographical conditions found there. In winter, a wide area with SO_4^{2-} concentrations larger than 10 $\mu g\ m^{-3}$ spread south and even expanded to 10°N, in accordance with changes in temperature and water contents along the transport path. In spring, higher SO_4^{2-} concentrations were found along the transport path from Hunan Province through Hubei Province to the convergence zone between 30°N and 40°N, and then the pollution was continually transported to the Yellow Sea, the Korean peninsula, and Japan. In summer, the SO_4^{2-} maximum was found in the Beijing-Tianjin-Hebei region, the Bay of the Bohai Sea, and Korea. Influenced by transportation from China, the concentration of SO_4^{2-} is highest in summer in most areas of Japan throughout the year (>10 $\mu g\ m^{-3}$). Under the effect of anticyclone circulations over central and eastern China, much of the pollutants in autumn were trapped in China, with a larger area of high SO_4^{2-} concentrations ($\geq$30 $\mu g\ m^{-3}$) existing over southern

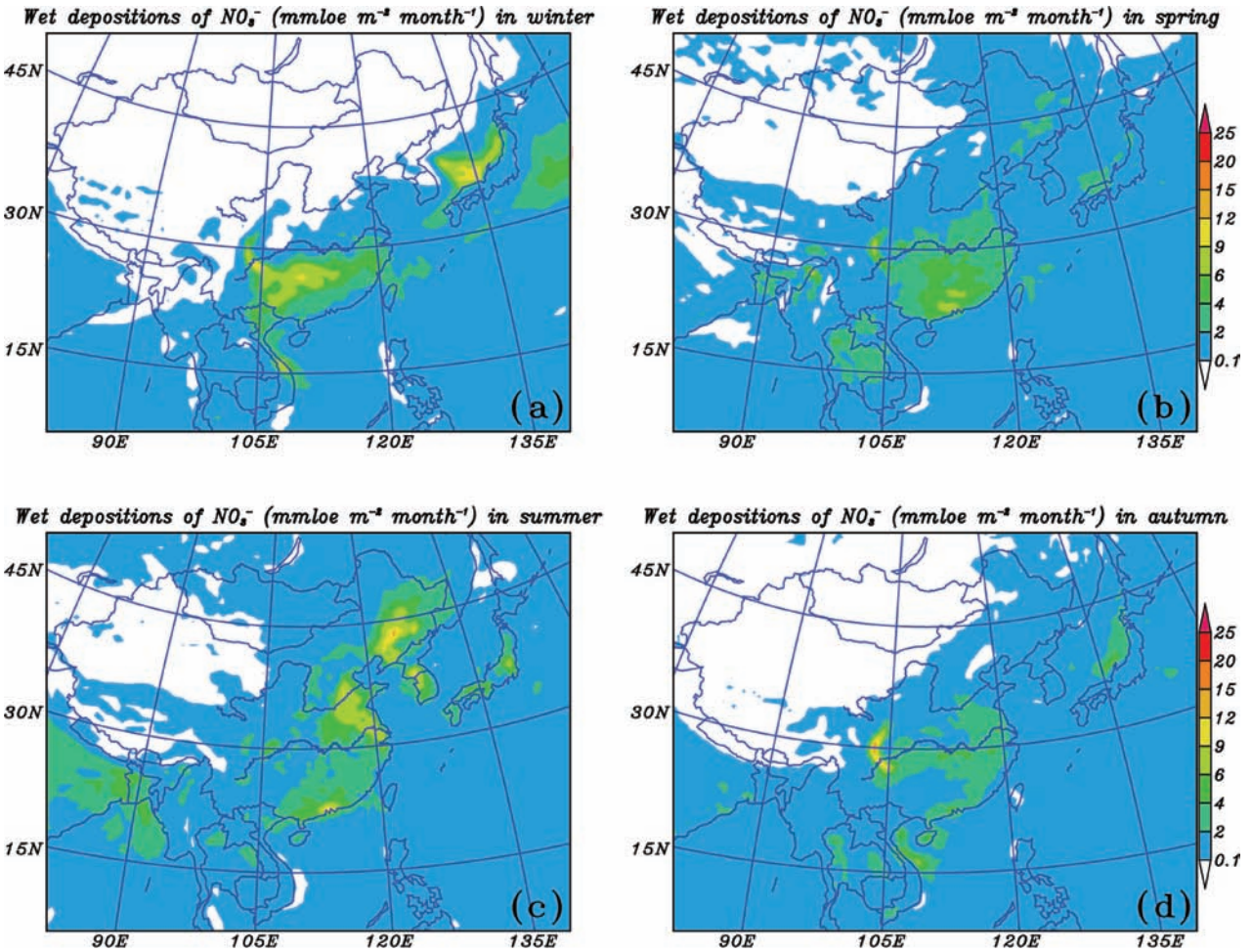

Figure 10. Modeled wet deposition fluxes (m mole m^{-2} $month^{-1}$) of NO_3^- in (a) winter (December–February), (b) spring (March–May), (c) summer (June–August), and (d) autumn (September–November) of 2005.

China and a small amount of SO_4^{2-} being transported to the West Pacific.

The higher NO_3^- concentrations were mainly found between the Yangtze River and the Yellow River throughout nearly the entire year because this area is characterized by high emissions of NO_x and NH_3. Because the concentration of NO_3^- is heavily influenced by temperature and precipitation, the NO_3^- concentrations have noticeable seasonal differences. The highest NO_3^- concentrations vary seasonally by a factor of approximately 4, with a maximum in winter $\geq$40 $\mu g\ m^{-3}$ and a maximum in summer $\geq$10 $\mu g\ m^{-3}$. Most regions of Asia have higher concentrations of SO_4^{2-} than NO_3^-, whereas the magnitudes of NO_3^- concentrations in some regions are slightly higher than concentrations of SO_4^{2-} (e.g., in eastern China and northeastern China in winter), suggesting an increased importance of NO_x emissions in these regions.

The spatial distributions of simulated wet deposition in East Asia in winter, spring, summer, and autumn clearly show that East Asia experiences noticeable wet deposition patterns during different seasons. In winter, southern China and the coastal areas of the Japan Sea demonstrate higher SO_4^{2-} and NO_3^- wet deposition levels. In spring, elevated SO_4^{2-} and NO_3^- wet deposition levels are found in northeastern China, southern China, and around the Yangtze River. In summer, a remarkable rise in precipitation in northeastern China, the valleys of the Huaihe and Yangtze rivers, Korea, and Japan leads to noticeable increases in SO_4^{2-} and NO_3^- wet deposition levels. In autumn, the higher SO_4^{2-} and NO_3^- wet deposition levels are found around Sichuan Province. Throughout the whole year, due to high emissions of SO_2, high SO_4^{2-} wet deposition levels are found in the area surrounding Sichuan Province.

Both observed and simulated results display a tendency toward decreasing values of NO_3^- and NH_4^+ mixing ratios in rainwater from China through Korea to Japan, indicating the influence of continental outflow from Eurasia. For all stations, except those in Banryu, the NO_3^- and NH_4^+ rainwater mixing ratios displayed much lower values in Japan than in Korea. This tendency was not observed for SO_4^{2-}.

Acid rain precipitated in most of Asia is still a typical sulfate-kind characterized by a higher wet deposition of SO_4^{2-} and a lower wet deposition of NO_3^-, although some areas are found to have higher levels of NO_3^- than SO_4^2, especially in the areas around the Taiwan Strait and the Tokyo district in winter.

ACKNOWLEDGMENTS

This study was supported by the National Basic research Program of China (2007CB407303) and the National Natural Science Foundation of China (20937001 and 41005064). The authors thank the Asia Center for Air Pollution Research (ACAP) in Japan for the data sets used in this study. Four anonymous reviewers are acknowledged for their careful reviews and constructive suggestions.

REFERENCES

1. Lefohn, A.S.; Husar, J.D.; Hasar, R.B. Estimating Historical Anthropogenic Global Sulfur Emission Patterns for the Period 1850–1990; *Atmos. Environ.* **1999**, *33*, 3435–3444.
2. Park, S.U.; Lee, Y.H.; Lee, E.H. Estimation of Nitrogen Dry Deposition in South Korea; *Atmos. Environ.* **2002**, *36*, 4951–4964.
3. Fu, J.S.; Jang, C.J.; Streets, D.G.; Li, Z.P.; Kwok, R.; Park, R.; Han Z.W. MICS-Asia II: Modeling Gaseous Pollutants and Evaluating an Advanced Modeling System over East Asia; *Atmos. Environ.* **2008**, *42*, 3571–3583.
4. Zhang, R.J.; Ho, K.F.; Cao, J.J.; Han, Z.W.; Zhang, M.G.; Cheng, Y.; Lee, S.C. Organic Carbon and Elemental Carbon Associated with PM10 in Beijing During Spring Time; *J. Hazard. Mater.* **2009**, *172*, 970–977.
5. Akimoto, H. Global Air Quality and Pollution; *Science*. **2003**, *302*, 1716–1719.
6. Tonooka, Y. Emission Inventory in Japan and East Asia. In *Proceedings of International Symposium on Emission Inventory and Prevention Technology for the Atmospheric Environment*, Tsukuba, Japan, 24–25 May 1992; pp 38–52.
7. Park, S.U. *Proceedings of International Conference on Acid Deposition in East Asia*, Taipei, Taiwan, 28–30 May 1996; pp 30–35.
8. Park, S.U.; In, H.J.; Kim, S.W.; Lee, W.H. Estimation of Sulfur Deposition in South Korea; *Atmos. Environ.* **2000**, *34*, 3259–3269.
9. Takahashi, A.; Fujita, S. Long-Term Trends in Nitrate to Non-Seasalt Sulfate Ratio in Precipitation Collected In Western Japan; *Atmos. Environ.* **2000**, *34*, 4551–4555.
10. Otoshi, T.; Fukuzaki, N.; Li, H.; Hoshino, H.; Sase, H.; Suzuki, K. Quality Control and Its Constraints During the Preparatory-Phase Activities of the Acid Deposition Monitoring Network In East Asia (EANET); *Water Air Soil Pollut.* **2001**, *130*, 1613–1618.
11. Schauer, J.; Mader, B.T.; Deminter, J.T.; Heidemann, G.; Bae, M.S.; Seinfeld, J.H.; Flagan, R.C.; Cary, R.A.; Smith, D.; Huebert, B.J.; Et Al. ACE-Asia Intercomparison of a Thermal-Optical Method for the Determination of Particle-Phase Organic and Elemental Carbon; *Environ. Sci. Technol.* **2003**, *37*, 993–1001; doi: 10.1021/Es020622f.
12. Seto, S.; Hara, H.; Sato, M.; Noguchid, I.; Tonookae, Y. Annual and Seasonal Trends of Wet Deposition in Japan; *Atmos. Environ.* **2004**, *38*, 3543–3556.
13. Carmichael, G.R.; Calori, G.; Hayami, H.; Uno, I.; Cho, S.Y.; Engardt, M.; Kim, S.-B.; Ichikawa, Y.; Ikeda, Y.; Woo, J.-H.; Ueda, H.; Amann, M. The MICS-Asia Study: Model Intercomparison of Long-Range Transport and Sulfur Deposition in East Asia; *Atmos. Environ.* **2002**, *36*, 175–199.
14. Park, S.U.; Lee, E.H. Long-Range Transport Contribution to Dry Deposition of Acid Pollutants In South Korea; *Atmos. Environ.* **2003**, *37*, 3967–3980.
15. Zhang, M.G.; Uno, I.; Yoshida, Y.; Xu, Y.F.; Wang, Z.Z.; Akimoto, H.; Bates, T.; Quinn, T.; Banddy, A.; Blomquist, B. Transport and Transformation of Sulfur compounds over East Asia during the TRACE-P and ACE-Asia Campaigns; *Atmos. Environ.* **2004**, *38*, 6947–6959.
16. Wang, Z.F.; Akimoto, H.; Uno, I. Neutralization of Soil Aerosol and its Impact on the Distribution of Acid Rain Over East Asia: Observations and Model Results; *J. Geophys. Res.* **2002**, *107* (D19), 4389; doi: 10.1029/2001JD001040.
17. An, J.L.; Ueda, H.; Wang, Z.F.; Matsuda, K.; Kajino, M. Simulations of Monthly Mean Nitrate Concentrations in Precipitation; *Atmos. Environ.* **2002**, *36*, 4159–4171.
18. Zhang, M.G.; Gao, L.J.; Ge, C.; Xu, Y. Simulation of Nitrate Aerosol Concentrations over East Asia with the model system RAMS-CMAQ; *Tellus*. **2007**, *59B*, 372–380.
19. Han, Z.W.; Ueda, H.; Matsuda, K. Model Study of the Impact Of Biogenic Emission on Regional Ozone and Effectiveness of Emission Reduction Scenarios over Eastern China; *Tellus*. **2005**, *53B*, 171–191.
20. Han, Z.W.; Ueda, H.; Matsuda, K.; Zhang, R.J.; Arao, K.; Kanai, Y.; Hasome, H. Model Study on Particle Size Segregation and Deposition during Asian Dust Events in March 2002; *J. Geophys. Res.* **2004**, *109* (D19205), pp. 1–19; doi: 10.1029/2004JD004920.
21. Zhang, M.G.; Uno, I.; Sugata, S.; Wang, Z.; Byun, D.; Akimoto, H. Numerical Study of Boundary Layer Ozone Transport and Photochemical Production in East Asia in the Wintertime; *Geophys. Res. Lett.* **2002**, *29*, 40-1-40-4; doi: 10.1029/2001GL014368.
22. Eder, B.; Shaocai, Y. An Evaluation of Model Performance of EPA Models-3/CMAQ. *Atmos. Environ.* **2006**, *40*, 4811–4824.
23. Zhang, M.G.; Uno, I.; Carmichael, G.R.; Akimoto, H.; Wang, Z.; Tang, Y.; Woo, J.H.; Streets, D.G.; Sachse, G.W.; Avery, M.A.; et al. Large-Scale Structure of Trace Gas and Aerosol Distributions over the Western Pacific Ocean during TRACE-P; *J. Geophys. Res.* **2003**, *108*, 40-1-40-19; doi: 10.1029/2002JD002946.
24. Zhang, M.G.; Uno, I.; Zhang, R.J.; Han, Z.W.; Wang, Z.F.; Pu, Y.F. Evaluation of the Models-3 Community Multi-scale Air Quality (CMAQ) Modeling System with Observations Obtained during the TRACE-P Experiment: Comparison of Ozone and its Related Species; *Atmos. Environ.* **2006a**, *40*, 4874–4882.
25. Zhang, M.G.; Pu, Y.F.; Zhang, R.J.; Han, Z.W. Simulation of Sulfur Transport and Transformation in East Asia with a Comprehensive Chemical Transport Model; *Environ. Model. Software*. **2006b**, *21*, 812–820.
26. Yarwood, G.; Rao, S.; Yocke, M.; Whitten, G. Updates to the Carbon Bond Chemical Mechanism: CB05, 2005. Final Report to the US EPA, RT-0400675. http://www.camx.com/publ/pdfs/CB05_Final_Report_120805.pdf. (accessed August 1, 2011).
27. Yu, S.; Bhave, P.V.; Dennis R.L.; Mathur R. Seasonal and Regional Variations of Primary and Secondary Organic Aerosols over the Continental United States: Observation-Based Estimates and Model Evaluation. *Environ. Sci. Technol.* *2007*, *41*, 4690–4697.
28. Pielke, R.A.; Cotton, W.R.; Walko, R.L.; Tremback, C.J.; Lyons, W.A.; Grasso, L.D.; Nicholls, M.E.; Moran, M.D.; Wesley, D.A.; Lee, T.J.; Copeland, J.H. A Comprehensive Meteorological Modeling System—RAMS; *Meteorol. Atmos. Phys.* **1992**, *49*, 69–91.
29. Kain, J.S. The Kain-Fritsch Convective Parameterization: An Update; *J. Appl. Meteorol.* **2004**, *43*, 170–181.
30. Walko, R.L.; Cotton, W.R.; Meyers, M.P.; Harrington, J.Y. New RAMS Cloud Microphysics Parameterization, Part I: The Single-Moment Scheme; *Atmos. Res.* **1995**, *28*, 29–62.
31. Mellor, G.L.; Yamada, T. A Hierarchy of Turbulence Closure Models for Planetary Boundary Layers; *J. Atmos. Sci.* **1974**, *31*, 1791–1806.
32. Lee, T.J. *The Impact of Vegetation on the Atmospheric Boundary Layer and Convective Storms*; Atmospheric Science Paper No 509; Department of Atmospheric Science, Colorado State University: Fort Collins, CO, 1992.
33. Streets, D.G.; Zhang, Q.; Wang, L.; He, K.; Hao, J.; Wu, Y.; Tang, Y.; Carmichael, G.R. Revisiting China's CO Emissions after the Transport and Chemical Evolution over the Pacific (TRACE-P) Mission: Synthesis of Inventories, Atmospheric Modeling, and Observations; *J. Geophys. Res.* **2006**, *111*, D14306; doi: 10.1029/2006JD007118.
34. Benkovitz, C.M.; Schultz, M.T.; Pacyna, J.; Tarrasón, L.; Dignon, J.; Voldner, E.C.; Spiro, P.A.; Logan, J.A.; Graedel, T.E. Global Gridded Inventories of Anthropogenic Emissions of Sulfur and Nitrogen; *J. Geophys. Res.* **1996**, *101*, 239–253.
35. Olivier, J.G.J.; Bouwman, A.F.; Maas, C.W.M.; Berdowski, J.J.M. Emission Database for Global Atmospheric Research; *Environ. Monit. Assess.* **1994**, *31*, 93–106.
36. Streets, D.G.; Bond, T.C.; Carmichael, G.R.; Fernandes, S.D.; Fu, Q.; He, D.; Klimont, Z.; Nelson, S.M.; Tsai, N.Y.; Wang, M.Q.; et al. An Inventory of Gaseous and Primary Emissions in Asia in the Year 2000; *J. Geophys. Res.* **2003**, *108* (D21), 8809.
37. Emmons, L.K.; Walters, S.; Hess, P.G.; Lamarque, J.-F.; Pfister, G.G.; Fillmore, D.; Granier, C.; Guenther, A.; Kinnison, D.; Laepple, T.; et al. Description and Evaluation of the Model for Ozone and Related chemical Tracers, version 4 (MOZART-4); *Geosci. Model Dev. Discuss.* **2009**, *2*, 1157–1213.
38. Ding, Y.H.; Liu, Y.M.; Shi, X.L.; Li, Q.Q.; Li, Q.P.; Liu, Y. Multi-Year Simulations and Experimental Seasonal Predictions for Rainy Seasons in China by Using a Nested Regional Climate Model (RegCM NCC) Part II: The Experimental Seasonal Prediction; *Adv. Atmos. Sci.* **2006**, *23*, 487–503.
39. Kato, H.; Hirakuchi, H.; Nishizawa, K.; Giorgi, F. Performance of NCAR RegCM2 in the Simulation of June and January Climate over Eastern Asia and High Resolution Effect of the Model; *J. Geophys. Res.* **1999**, *104*, 6455–6476.
40. Lee, D.K.; Suh, M.S. Ten-Year Asian Summer Monsoon Simulation Using a Regional Climate Model (RegCM2); *J. Geophys. Res.* **2000**, *105*, 29565–29577.
41. Small, E.E.; Giorgi, F.; Sloan, L.C. Regional Climate Model Simulation of Precipitation in Central Asia: Mean and Interannual Variability. *J. Geophys. Res.* **1999**, *104*, 6563–6582.
42. Leung, L.R.; Ghan, S.J.; Zhao, Z.C.; Luo, Y.; Wang, W.C.; Wei, H.L. Intercomparison of Regional Climate Simulations of 1991 Summer Monsoon in Eastern Asia; *J. Geophys. Res.* **1999**, *104*, 6425–6454.
43. Matsumoto, K.; Uyama, Y.; Hayano, T.; Tanimoto, H.; Uno, I.; Uematsu, M. Chemical Properties and Outflow Patterns of Anthropogenic and Dust Particles on Rishiri Island during the Asian Pacific Regional Aerosol Characterization Experiment (ACE-Asia); *J. Geophys. Res.* **2003**, *108* (D23), 8666; doi: 10.1029/2003JD003426.
44. Carmichael, G.R.; Zhang, Y.; Chen, L.L.; Hong, M.S.; Ueda, H. Seasonal Variation of Aerosol Composition at Cheju Island, Korea; *Atmos. Environ.* **1996**, *30*, 2407–2416.

45. Yamamoto, N.; Kabeya, N.; Onodera, M.; Takahahi, S.; Komori, Y.; Nakazuka, E.; Shirai, T. Seasonal Variation of Atmospheric Ammonia and Particulate Ammonium Concentrations in the Urban Atmosphere of Yokohama over a 5-Year Period; *Atmos. Environ.* **1988**, *22*, 2621–2623.
46. Wang, W.X.; Wang, T. On the Origin and the Trend of Acid Precipitation in China; *Water Air Soil Pollut.* **1995**, 85, 2295–2300.
47. Yu, S.C.; Dennis, R.; Roselle, S.; Nenes, A.; Walker, J.; Eder, B.; Schere, K.; Swall, J.; Robarge, W. An Assessment of the Ability of Three-Dimensional Air Quality Models with Current Thermodynamic Equilibrium Models to Predict Aerosol NO_3. *J. Geophys. Res.* **2005**, *110*, 1–13 (D07S13), xx; doi: 10.1029/2004JD004718.
48. Zhang, Y.; Liu, P.; Queen, A.; Misenis, C.; Pun, B.; Seigneur, C.; Wu, S.Y. A Comprehensive Performance Evaluation of MM5-CMAQ for the Summer 1999 Southern Oxidants Study Episode—Part II: Gas and Aerosol Predictions; *Atmos. Environ.* **2006**, *40*, 4839–4855.
49. Carmichael, G.R.; Uno, I.; Phadnis, M.J.; Zhang, Y.; Sunwoo,Y. Tropospheric Ozone Production and Transport in the Springtime in East Asia; *J. Geophys. Res.* **1998**, *103*, 10649–10671.
50. Ikeda, Y.; Higashino, H. The Estimation of Acid Deposition in East Asia (II)— Focused on the Ratio of Sources Contribution of the Deposition; *J. Japn. Soc. Atmos. Environ.* **1997**, *32*, 175–186.
51. Ichikawa, Y.; Hayami, H.; Fujita, S. A Long-Range Transport Model for East Asia to Estimate Sulfur Deposition in Japan; *J. Appl. Meteorol.* **1998**, *37*, 1364–1974.

About the Authors

Dr. Cui Ge is a research fellow at Institute of Atmospheric Physics, Chinese Academy of Sciences. Dr. Meigen Zhang is a professor at Institute of Atmospheric Physics, Chinese Academy of Sciences. Ms. Lingyun Zhu is a senior engineer at Shanxi Province Meteorological Institute. Dr. Xiao Han is a research fellow at Institute of Atmospheric Physics, Chinese Academy of Sciences. Dr. Jun Wang is an assistant Professor at Department of Earth and Atmospheric Sciences, University of Nebraska – Lincoln. Please address correspondence to: Meigen Zhang, Institute of Atmospheric Physics, Chinese Academy of Sciences, 40# HuaYanLi, ChaoYang District, Beijing, China, 100029; phone: +86-10-62379620; fax: +86-01-62041393; e-mail mgzhang@mail.iap.ac.cn.